Kinetics of radiation-induced DNA double-strand breaks through coarse-grained simulations

Manuel Micheloni,[1] Lorenzo Petrolli,[1,2] Gianluca Lattanzi,[1,2] and Raffaello Potestio[1,2,*]

[1] *Department of Physics, University of Trento, Via Sommarive 14, I-38123 Trento, Italy*
[2] *INFN-TIFPA, Trento Institute for Fundamental Physics and Applications, I-38123 Trento, Italy*

(Dated: July 3, 2022)

The DNA lesions enforced by the collision of the radiation field with the cell nucleus involve a variety of local, mostly reversible, mutations of the DNA template. Yet, the double strand break (DSB) of the DNA backbone is reckoned to be the most detrimental outcome of cell irradiation, bearing a non-negligible likelihood of chromosomal aberrations and cell apoptosis from the failure of the DNA damage response (DDR) machinery. In the early stages of the evolution of a DSB lesion, the DNA moieties likely drift from a metastable, bound state, thereby achieving a fracture of the helical layout: arguably, the thermal disruption of the residual interactions at the interface of a DSB lesion drives the rupturing process, despite its kinetics being poorly characterized both *in vitro* and *in silico*. Here, we address the characterization of the mechanical fracture of DSB motifs by means of molecular dynamics, employing a coarse-grained DNA model. The setup involves a steered 3855-bp DNA filament, resembling an optical tweezing experiment. Strand breaks are enforced within a range of distances between 0 and 4 base pairs, and the subsequent dislocation of the broken DNA moieties is tracked, accounting for the molecular details and the characteristic timescales of the rupturing process. A linear correlation is observed between the DSB distance (i.e. between strand breaks of the DNA backbone) and the height of the internal energy barrier of the process, separating the bound and fractured states of the DNA filament. Moreover, we infer an exponential dependence of the average fracture times with the DSB distances, thus allowing us to model the DSB event as an activated process following an Arrhenius-Kramers law. This work lays the foundations of a detailed, mechanistic assessment of DSB lesions *in silico*, as well as of a direct benchmark between numerical simulations and data from single molecule experiments.

I. INTRODUCTION

DNA holds the hereditary information required by cells to replicate and carry out their biological activity. Cells, however, are constantly threatened by a variety of toxic agents, of both *endogenous*, i.e. naturally associated with a cell life-cycle, e.g. as by-products of metabolic stresses [1] and DNA replication [2], and *exogenous* origin, such as chemicals and ionizing radiations (IR) [3, 4]. In fact, IR accounts for a variety of chemical and mechanical lesions of the DNA molecule, involving a wide range of resolution and time scales, which are mediated by a cascade of inelastic collisions and radiolytic reactions [5]. Amongst the plethora of radiation-enforced DNA lesions, however, the disruption of the phosphoester backbone over both DNA strands, or double strand break (DSB), is arguably the most toxic [3]. In fact, DSBs account for major cytotoxic effects, and critically so at sites of highly-condensed lesions within localized DNA volumes [6, 7]; indeed, lesion clustering is a striking lethal feature of IR at high linear energy transfer regimes, i.e. associated with a massive release of energy at the microscale [8, 9]. The processing, and subsequent repair, of DNA lesions add a further layer of complexity: cross-regulated cell defense mechanisms are deployed as a DNA lesion is sensed, thereby recruiting a dedicated enzymatic framework *in situ via* a cascade of signaling pathways, overall referred to as the DNA damage response (DDR) [3, 10, 11]. In the context of the DDR, eukaryotic cells employ two major, competitive responses to tackle DSBs: a homology-dependent pathway, which is active in the pre-mitotic stage of the cell-cycle (or the homologous recombination, HR), and a ubiquitous, homology-independent pathway (or the non-homologous end joining, NHEJ). The choice between HR and NHEJ (as well as alternate minor routes) reflects directly upon the kinetics and outcome of the DDR activity, and might underlie collateral processing errors affecting its accuracy [10, 12–14]. In fact, a negative outcome from the repair of a DSB lesion is associated with several detrimental and cytotoxic consequences, such as modifications in the expression of genes and gene mutations, chromosomal aberrations, genomic instabilities, and apoptosis.

Numerical simulations have offered key insights on the behavior of DNA lesions at all significant scales of the chromatin framework, detailing the process at high-resolution levels mostly inaccessible by conventional experimental techniques *in vitro* and *in vivo*. The radial distribution of the events of energy release about a radiation track is assessed *in silico* by means of Monte Carlo track structure (MCTS) codes, which depict the event-by-event evolution of the physical and chemical interactions between a radiation carrier and the target tissue [15–18]. Moreover, effective criteria have been developed to associate the layout of the radiation track to the occurrence of local DNA modifications within significant sub-cellular volumes, thereby providing a static

* raffaello.potestio@unitn.it

picture of the early distribution of DNA lesions at the micro- and nanoscale [17, 19–21]. In a few cases, realistic cell-like scenarios involve the kinetics of the DDR activity [22–24], to achieve system-specific rates that reflect the average signaling and processing by the enzymes involved with a given pathway. Overall, these methods tackle the description of the outcomes from the irradiation of cells *via* a mean field approach, whereby various realisations of the track path and/or of the cell response are averaged. Yet, a mechanistic framework of the local dynamics of chromatin, at the earliest stages of the (radiation-enforced) DNA damage, is critical in the context of the DDR.

The DNA rupture, whereby the disjointed DNA termini drift from the lesion site, unfolds by a sub-diffusive dynamics, i.e. the mean square displacement of the DSB moieties is associated with a non-linear dependence with time [25]. This regime is accounted for by the effective constraints enforced by both the nuclear *milieu* and the supramolecular association of DDR enzymes, such as the Ku heterodimer or the RAD51 recombinase [26, 27]. The sub-diffusion of DNA termini has been depicted *in silico* (in the framework of MCTS codes) by biasing the Brownian dynamics of the broken DNA moieties in a continuous, effective medium [24, 28, 29]. However, the theoretical framework underneath MCTS overlooks the dynamical detail to characterize DSBs at the molecular level, i.e. the forces driving the dynamics of DNA are involved implicitly by means of empirical coefficients.

A complementary insight might be offered by molecular dynamics (MD) techniques, evolving the dynamical behavior of DSBs over single DNA molecules, and eventually laying the groundwork to correlate the features of the DSB motifs and the choice of the DDR pathway. Landuzzi and co-workers [30] have assessed the thermal and forceful fracture of DSBs on a short 31-bp DNA sequence depicting a DNA *linker* (that is, the exposed, linear DNA stretch between nucleosomes in a chromatin fiber) *via* atomistic MD. Notably, they inferred that the direct observation of fractures in the DNA backbone beyond a DSB distance of 3-bp is unlikely within the time scales associated with the activity of the DDR. However, it is broadly acknowledged that atomistic force fields of nucleic acids might over-estimate the strength of the non-covalent forces holding the DNA molecule (such as π-stacking contacts) [31, 32], thus slightly biasing the equilibrium dynamics of DNA assemblies. Moreover, atomistic MD assessments are bound by a significant numerical overhead, so that the accessible dynamics of biological systems is restricted to a few microseconds and/or a few replicas. These limitations may be circumvented by exploiting coarse-grained (CG) models, where groups of atoms are specifically mapped into a lower resolution description of the system. The CG sites interact by means of effective potentials, derived from either *top-down* or *bottom-up* approaches [32]; remarkable examples of CG models of DNA are MARTINI [33], 3SPN [34] and oxDNA [35]. Notably, the oxDNA force-field has been widely acknowledged to reliably depict systems that are relevant in DNA nanotechnology, such as DNA origami [36], for extended timescales.

In this work, we assessed the rupturing process of DNA driven by double strand break lesions, described at a CG level *via* the oxDNA force field. To this aim, we enforced DSBs of the DNA backbone (or T1-DSBs, as defined by Schipler and Iliakis [3]), at distances ranging between 0 and 4 bp, on a 3855-bp DNA molecule, depicting the optical-tweezing (OT) experimental setup of Wang and co-workers [37]. We performed extensive MD simulations, tracking the dynamics of the fractured DNA moieties and the kinetics of the subsequent rupturing process, which is driven by the disruption of all residual contacts holding the helical framework. In all DSB scenarios, we kept the DNA molecule at varied steered end-to-end distances by a coaxial force. Moreover, extra care was dedicated to the definition of time in CG dynamics, by effectively scaling the observed fracturing kinetics upon the diffusion coefficients of DNA - as estimated from experimental and computational assessments of freely-diffusing DNA molecules. We thus modeled the DSB fracturing event as an activated process, thereby following an Arrhenius-Kramers law: we estimated the activation free energies associated to different DSB motifs and established an effective correlation with the average rupture times. Lastly, we extrapolated the kinetics of the dislocation of DSBs at distances between 5 to 10-bp, which is hardly accessible *in silico* at the level of theory of the oxDNA force field.

II. MATERIALS AND METHODS

A. The oxDNA coarse-grained model

We simulated a 3855-bp, double-stranded DNA filament in the B-conformation employing the oxDNA2 coarse-grained (CG) force field, which has been acknowledged to reproduce faithfully both mechanical and thermodynamic properties of DNA [35, 38, 39]: it improves on the earlier oxDNA model, introducing effective temperature- and sequence-dependent stacking and electrostatic interactions, thereby refining the behaviour of DNA in implicit solvent and different ionic concentrations, down to physiological conditions [40]. Moreover, the level of resolution associated with oxDNA2 is adequate to detail the local dynamical features of DSB lesions while lowering the numerical overhead of the atomistic force fields, hence covering time-frames that are biologically significant [32, 41]. It is worth noting that, while the oxDNA2 force field is benchmarked upon experimental, equilibrium properties of DNA, as well as higher-resolution calculations, we hereby assess non-equilibrium processes - so that its validity has to be verified *a posteriori*.

OxDNA2 employs Lennard-Jones (LJ) reduced units and, despite the conversion between units being straight-

forward [41], specific care has to be paid to the definition of time. In fact, it is well-acknowledged that CG models accelerate the dynamics of physical processes in a non-trivial manner [42]; we require a rule to recover the proper definition of time, which will be further discussed throughout this work. We will thus denote with τ the LJ time units associated with the CG dynamics of DNA, while keeping the classical SI notation to refer to the properly rescaled characteristic times of the dynamical processes.

B. Molecular dynamics simulations

MD simulations were carried out on the LAMMPS software platform [43, 44]. The dynamics of the DNA molecule was assessed in the NVT ensemble at $T = 310$ K and a monovalent ionic strength of 0.15 M, to match a physiological environment. All simulations were performed employing the rigid-body Langevin-type integrator (Langevin C) [45], which solves the equations of motion accounting for an implicit solvent background. This integrator has shown enhanced performances, in contrast with the standard LAMMPS Langevin algorithm for DNA simulations, allowing a stable integration of the equations of motion at larger time steps [41, 46] - which we set to $\Delta t = 5 \times 10^{-3}$ τ, together with a damping coefficient of the Langevin thermostat ζ of 10 τ. Unless specified otherwise, this choice was employed in all simulations.

C. Simulation setup

The exact size of the 3855-bp double-stranded DNA filament has been chosen to roughly match those employed in the experimental, optical tweezing-setup of Wang and co-workers [37]. Thus, we enforced a step-wise thermalization protocol as follows: i) we let the DNA molecule relax at $T = 273$ K, until reaching a plateau of the total energy of the system; ii) we heated the system to the working temperature of $T = 310$ K in a quasi-static manner, by performing a single run of 1.6×10^5 τ in the NVT ensemble, associated with a damping coefficient ζ of 10 τ; iii) we ran a 3.3×10^5 τ simulation employing an underdamped Langevin thermostat ($\zeta = 100$ τ), to relax the molecule into an equilibrated conformation.
To achieve a configuration representative of an OT setup, we carried out several instances of steered MD simulations, thereby relaxing the DNA molecule at different elongation ratios: specifically, we set the end-to-end distance at $R_{ee} = 1000$, 1100, 1200, 1300 nm, to cover the behavior of the DNA chain about the mid-high region of the force-extension curve [37]. These conformations were obtained by employing two harmonic potentials restraining the termini of the chain, with associated elastic constants of $k_1 = 5.7$ N/m and $k_2 = 2.3 \times 10^{-3}$ N/m respectively, and by setting $\zeta = 10$ τ. This combination of parameters allowed us to slowly stretch the thermalized DNA molecule into each of the target end-to-end distances. Upon reaching the desired DNA conformation, we performed two equilibration stages of i) 4.9×10^4 τ with $\zeta = 100$ τ, and ii) 5.8×10^5 τ with $\zeta = 10$ τ. The four elongated configurations of DNA served as initial frames for a set of production runs aimed at assessing the early effects of DSBs.
As the radiation-enforced lesions of DNA bear several levels of complexity, varying upon the resolution scale [3, 17], a simplified, effective framework to assess DNA fractures is adopted that both depicts the process faithfully and is computationally feasible. In view of this, we focused on the T1-DSB type of damage, as described by Schipler and Iliakis [3], whereby IR simply induces the disruption of the phosphoester bonds of the DNA backbone. We thus neglected all modifications that involve the nitrogenous bases and only allowed thermal fluctuations to separate the DNA moieties. We hereby define the distance between breaks of the DNA backbone on complementary strands b_d (or **DSB distance**), as the amount of intact base pairs in-between the twofold breakage associated with a DSB lesion (Fig. 1). To enforce a DSB, we removed the covalent bonds between adjacent nucleotides on both DNA strands at distances $b_d = 0$, 1, 2, 3 and 4, about half-way of the DNA filament, to assess different DSB motifs. For each value of b_d, different replicas were run, starting from the same initial configurations but associated with different thermostat seeds, i.e. with different velocities of the CG beads. We remark that no prior minimisation/thermalization protocol of the DSBs was carried out, to depict the subsequent dynamics of a DNA molecule broken abruptly by the radiation field. A snapshot of an MD simulation of a DSB at $b_d = 1$ is reported in Fig. 1.

D. Derivation of the characteristic times of the DSB rupture

The characteristic time associated with the drifting of the DNA moieties from the lesion site, or **breaking time** τ_{b_d}, was estimated for each (b_d, R_{ee}) DSB scenario *via* a two-step procedure. First, we employed a geometrical, heuristic criterion to unequivocally characterize the DSB (Fig. 1B - see details in the Supplementary Data); the specific choice was corroborated by the visual analysis of the MD trajectories, so that we could concentrate on a time interval about the fracturing event. Thus, we derived τ_{b_d} from the internal energy profile of the nucleotides involved with the residual contact interface of a DSB motif: Fig. 2 shows the internal energy contribution of the contact nucleotides of a DSB at $b_d = 0$, within a time span involving the fracture of the DNA molecule. By assuming that the internal energy barrier dividing the two thermodynamic basins is symmetrical at the peak, we performed a sigmoidal fit on the internal energy profile and derived the characteristic time of the

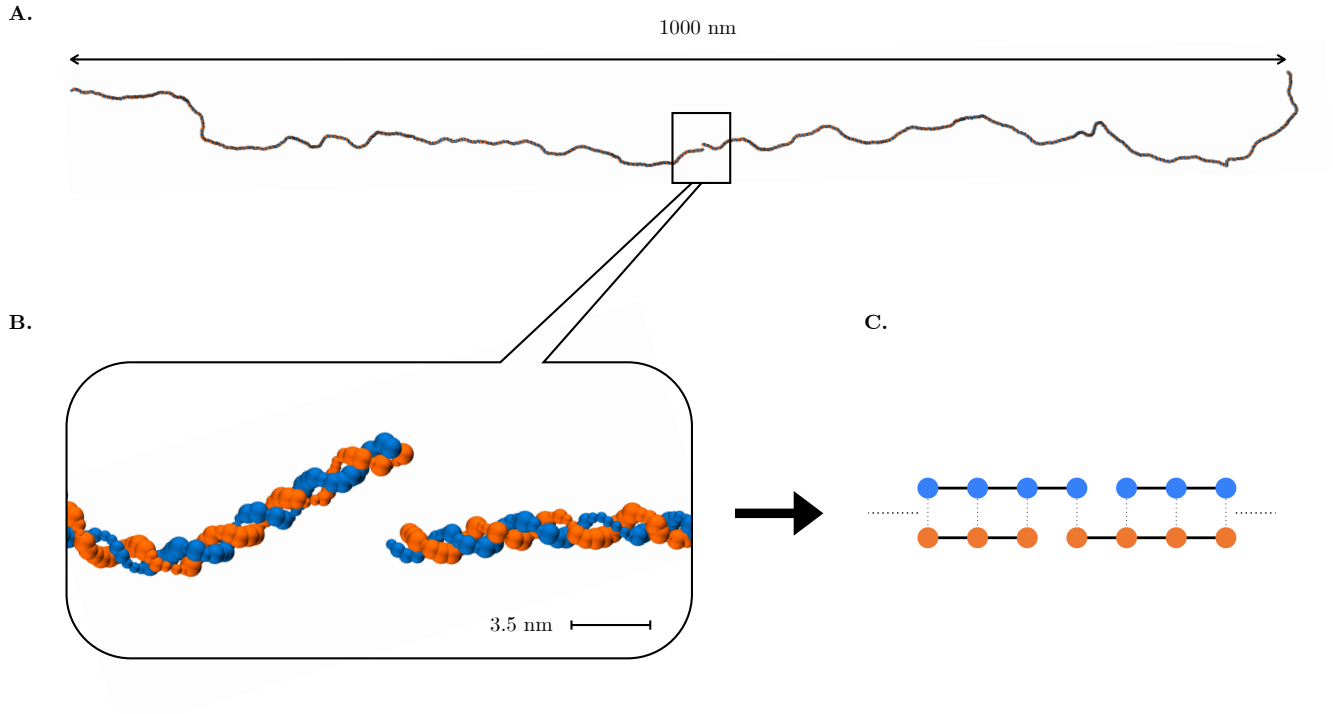

FIG. 1: (**A**) Snapshot of the 3855-bp B-DNA molecule, associated with an end-to-end distance of $R_{ee} = 1000$ nm, damaged by a double strand break at distance $b_d = 1$, shown in detail in the inset **B**. (**C**) Schematic representation of a DNA double strand break. Covalent bonds of the DNA backbone are represented as solid lines, hydrogen bonds between DNA strands as dotted lines. To enforce a DSB, covalent bonds are removed from both DNA strands.

DSB rupture, corresponding to the flex of the sigmoidal curve. Moreover, we estimated the internal energy barrier (ΔU) of the process as the energy difference between the flex point and the energy plateau of the bound state, which we will later associate with the transition state of the DNA rupture ($\Delta U^{\ddagger}$). Additional and technical details about the fitting procedure are reported in the Supplementary Data.

E. Correlation between physical time and simulation time in CG models

It is well acknowledged that CG models enhance the dynamics of systems with respect to their all-atom counterparts [32, 42, 47]. This is inherent to the integration of several degrees of freedom, whereby the coarse-graining procedure smoothens the free energy landscape, thus favoring the transition between local minima. Furthermore, CG models are typically employed in MD simulations in implicit solvents, which lack a proper characterization of the hydrodynamic effects associated with the collective motion of the solute particles nearby [38, 48]. These limitations only marginally affect the depiction of the structural features of a system at equilibrium [37, 49]. However, they become critical in the assessment of time-dependent, non-equilibrium kinetic observables. Under the assumption that the modifications induced by the coarse-graining procedure are reducible to a global redefinition of the characteristic times of a system [42], these issues may be tackled by rescaling the time steps of the CG simulation to match the outcome from a reference scenario, such as all-atom MD or wet lab experiments. In this view, we related the timescales of the physical (experimental) process and those of its *in silico* (CG) depiction *via* the ratio of diffusion coefficients of DNA, $\Gamma(\zeta)$ as:

$$t = \Gamma(\zeta)\, t_{\mathrm{CG}} = \frac{D_{\mathrm{CG}}(\zeta)}{D_{\mathrm{EXP}}} t_{\mathrm{CG}} \tag{1}$$

where t is the best estimate of the physical time, t_{CG} is the CG simulation time, and $D_{\mathrm{CG}}(\zeta)$ and D_{EXP} are the coarse-grained and the experimental diffusion constants respectively.

To estimate the value of $D_{\mathrm{CG}}(\zeta)$ of the 3855-bp DNA molecule, we performed 8 independent simulations of 4.7×10^5 τ starting from the equilibrated 1000 nm-conformation of DNA (from the steering protocol) in the NVT ensemble at $T = 310$ K, employing a friction coefficient $\zeta = 10\ \tau$, where the DNA molecules were allowed to diffuse freely. $D_{\mathrm{CG}}(\zeta)$ was thus inferred from a linear fitting of the average mean-squared displacement versus time (see Supplementary Data), whereby we achieved $D_{\mathrm{CG}} = 2.04 \times 10^{-10}\ \mu\mathrm{m}^2/\tau$.

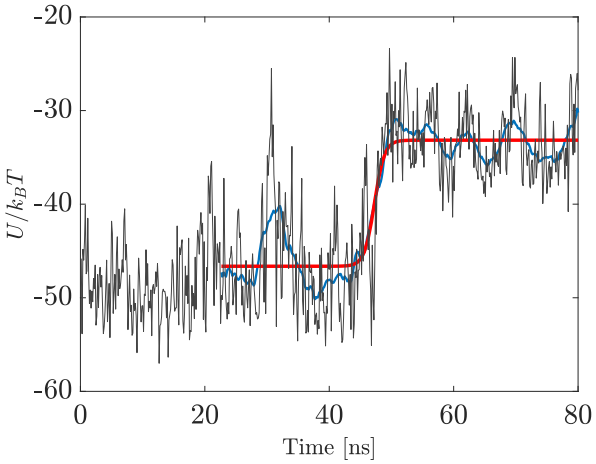

FIG. 2: Profile of the local internal energy contribution associated with the dislocation of a DSB motif, at distance $b_d = 0$ and steered end-to-end distance $R_{ee} = 1000$ nm. The lesion destabilizes the helical layout, thus allowing the DNA molecule to undertake a transition from a bound (metastable) to a dislocated (stable) state. The moving average of the potential energy profile (blue line) is fitted *via* a sigmoid curve (red line), whereby we assess the characteristic time and internal energy barrier of the DSB fracture.

As for D_{EXP}, we relied on the experimental procedure of Robertson and co-workers [50], who obtained the diffusion coefficient of λ-phage DNA fragments of different sizes, by coupling the action of the restriction enzyme HindIII (NEB) and gel electrophoresis. We thus extrapolated the value of D_{EXP} from the experimental diffusion coefficients of longer DNA filaments, and corrected it by the ratio of the temperatures adopted in our simulations and in the experimental setup, obtaining $D_{\mathrm{EXP}} = 1.17\ \mu\mathrm{m}^2/\mathrm{s}$ and a time-scaling conversion coefficient $\Gamma(\zeta)$ of 103.

III. RESULTS

We applied our proposed protocol to estimate the characteristic times associated with the fracture of a T1-DSB, assessing both the mechanical details and kinetics of the rupturing event.

A. Analysis of the residual interactions at the characteristic time of a DSB rupture

After a DNA molecule is nicked by a T1-DSB, the residual, non-covalent interactions between DNA moieties alone stabilize the helical layout, thereby preventing the further disruption of the molecule. In fact, the twofold removal of covalent bonds at the DNA backbone triggers the destabilization of the structure, driven by the Coulombic repulsion between adjacent nucleotides at the breakage interface; yet, the residual hydrogen bonds and stacking contact interactions temporarily hold the integrity of the DNA helix. However, as all non-bonded interactions between DNA moieties are disrupted, a shift in the internal energy of the system is observed (shown in Fig. 2).

We thus tracked the behaviour of all binary distances $r_{i,j}$ between the nucleotides involved at the DSB site (which ultimately embed effective non-covalent interactions) by means of three statistical estimators, and introduced *ad hoc* matrices quantifying the status of all effective interactions at the time of the fracturing event. The first estimator, $E_1(r_{i,j})$, is defined as:

$$E_1(r_{i,j}) = \frac{\left\langle r_{i,j}(b_d, R_{ee})|_{\tau_{b_d}} \right\rangle}{\langle r_{i,j}(b_d, R_{ee})\rangle^*} \tag{2}$$

where we employ the average distance between i, j nucleotide pairs at the fracture time at the numerator. We refer to the plain $\langle\cdot\rangle$ notation implying an averaging procedure over all independent (b_d, R_{ee}) simulations, whereas the $\langle\cdot\rangle^*$ notation is limited to configurations of the metastable, bound state. The second estimator, $E_2(r_{i,j})$:

$$E_2(r_{i,j}) = \frac{\sqrt{\left\langle \left[r_{i,j}(b_d, R_{ee})|_{\tau_{b_d}} - \langle r_{i,j}(b_d, R_{ee})\rangle^* \right]^2 \right\rangle}}{\sqrt{\left\langle \left[r_{i,j}(b_d, R_{ee}) - \langle r_{i,j}(b_d, R_{ee})\rangle^* \right]^2 \right\rangle}} \tag{3}$$

quantifies the fluctuations of the binary distances between nucleotides at the rupturing times (numerator) and in the bound state (denominator). Lastly, the third estimator, $E_3(r_{i,j})$, is a combination of $E_1(r_{i,j})$ and $E_2(r_{i,j})$:

$$E_3(r_{i,j}) = \frac{\sqrt{\left\langle \left[r_{i,j}(b_d, R_{ee})|_{\tau_{b_d}} - \langle r_{i,j}(b_d, R_{ee})\rangle^* \right]^2 \right\rangle}}{\left\langle r_{i,j}(b_d, R_{ee})|_{\tau_{b_d}} \right\rangle}. \tag{4}$$

Fig. 3 shows an example matrix collecting all binary estimators associated with a DSB at $b_d = 1$ and $R_{ee} = 1000$ nm (the matrices of all combinations of DSB motifs and end-to-end extensions are found in the Supplementary Data). For all (b_d, R_{ee}) simulation sets, the data obtained from Eq. 2 highlight that all binary distances increase by the rupturing time, at least two times their average value in the bound state. Overall, we observed that the distances between nucleotides involved with stacking interactions at the contact interfaces are always associated with the highest scoring estimators.

Regarding Eqs. 3 and 4, the fluctuations of the binary distances at τ_{b_d} are generally larger than those of the metastable state, as expected. Namely, hydrogen bonds

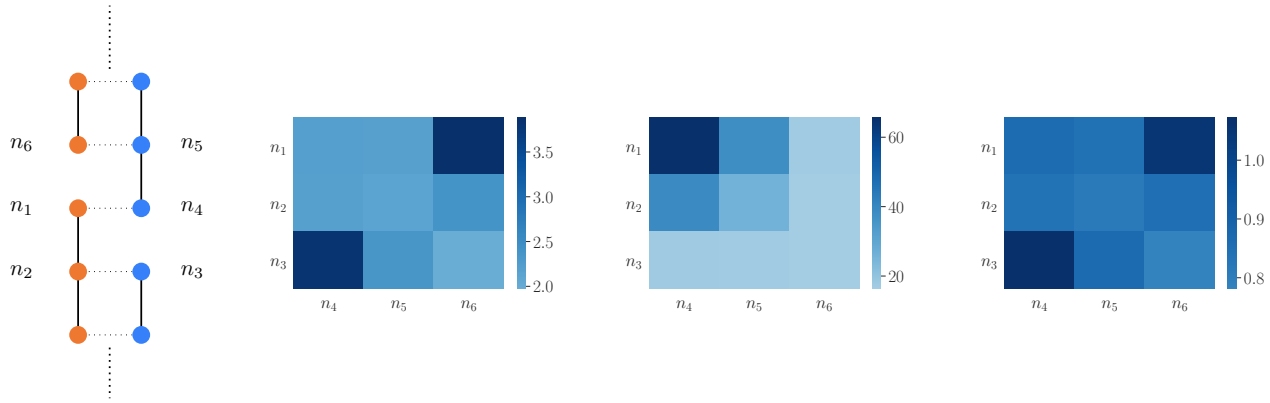

FIG. 3: Matrices of the binary estimators detailing the effective interactions between nucleotides, associated with the contact interface of a DSB motif at distance $b_d = 1$ and steered end-to-end distance $R_{ee} = 1000$ nm (an outline of the DSB interface is shown on the left). In the sequence, results obtained from Eq. 2, 3 and 4 are reported respectively (details in the text).

vary significantly about the rupture time in all DSB scenarios; in fact, the fluctuations of hydrogen-bonded nucleotides in the bound state are about five times lower than those of the stacking interactions. Lastly, the matrix associated with $E_3(r_{i,j})$ highlights that the magnitude of the fluctuations of all binary distances is significant and comparable to their average values in the metastable state.

B. Fracture kinetics of the DSB motifs

As a subsequent step, we assessed the influence of the DSB distance b_d on the fracture kinetics of the T1-DSB motifs, by estimating the average fracture time $\bar{\tau}_{b_d}$ over all independent simulations associated with a given (R_{ee}, b_d) combination. Results are outlined in Table I, where the characteristic times were scaled according to the protocol described earlier (see Materials and Methods). We thus analyzed the dependence of the average rupture times on the distance b_d of the different DSB motifs, by employing an exponential fitting law as:

$$\bar{\tau}_{b_d} = A \exp\left[-B b_d\right] \tag{5}$$

with A and B fitting coefficients - the results of the fitting procedure are reported in Table II. Indeed, Fig. 4 hints at the existence of an exponential relationship between the two observables, in spite of the error bars being significant at higher distances. This is in line with the work of Sengar and co-workers, who simulated the dissociation kinetics of duplexes 4-, 5- and 6-bp at 320 K, employing an earlier version of the oxDNA force-field [41]. Therefore, we focused on the relationship between the internal energy barrier associated with the DSB fracturing process and the DSB distance b_d. We assessed DSB motifs at distances shorter than the helical pitch of DNA (about 10 nucleotides), and performed a linear fitting procedure as:

$$\frac{\Delta U(b_d)}{k_B T} = \alpha b_d + \beta \tag{6}$$

with α and β fitting coefficients - reported in Table III for each R_{ee} distance. In fact, the validity of this assumption, i.e. the existence of a linear correlation between the internal energy barrier of the fracturing process and the DSB distance, is verified for all steered conformations, as shown in Fig. 5.

C. Mechanistic inferences on the DSB fracture kinetics

Once the structure of the DNA double helix has been compromised by a DSB event, non-covalent interactions hold the broken DNA moieties, thereby inhibiting the transition from a bound to a fractured state. As a consequence, the system is confined to a metastable state, until the kinetic barrier associated with the dislocation of the residual contact interface about the DSB site is overcome by means of stochastic thermal fluctuations, thus allowing the DNA molecule to reach a state of local thermodynamic equilibrium. This is an activated process, well described by the transition state theory [51–54]: a system progresses between metastable conformational basins, across a dynamical bottleneck enforced by the transition state. The status of the process may thus be tracked along a proper reaction coordinate, whereby reactive (reversible) trajectories are typically sampled by means of enhanced MD techniques.

TABLE I: Average rupture times $\bar{\tau}_{b_d}$ of the different DSB motifs and steered DNA extensions. Each $\bar{\tau}_{b_d}$ is determined by averaging over all independent simulations associated with a (b_d, R_{ee}) combination (whose amount is reported in brackets). The characteristic times are scaled according to Eq. 1. In all cases, the standard deviations are on the order of the average value.

R_{ee} [nm]	$\bar{\tau}_0$ [ns]	$\bar{\tau}_1$ [ns]	$\bar{\tau}_2$ [μs]	$\bar{\tau}_3$ [μs]	$\bar{\tau}_4$ [μs]
1000	82 (928)	549 (793)	9.0 (80)	10 (49)	54 (4)
1100	75 (913)	424 (869)	8.0 (95)	13 (48)	110 (5)
1200	78 (922)	525 (888)	7.2 (91)	14 (61)	110 (7)
1300	62 (884)	334 (846)	3.1 (288)	3.5 (227)	16 (49)

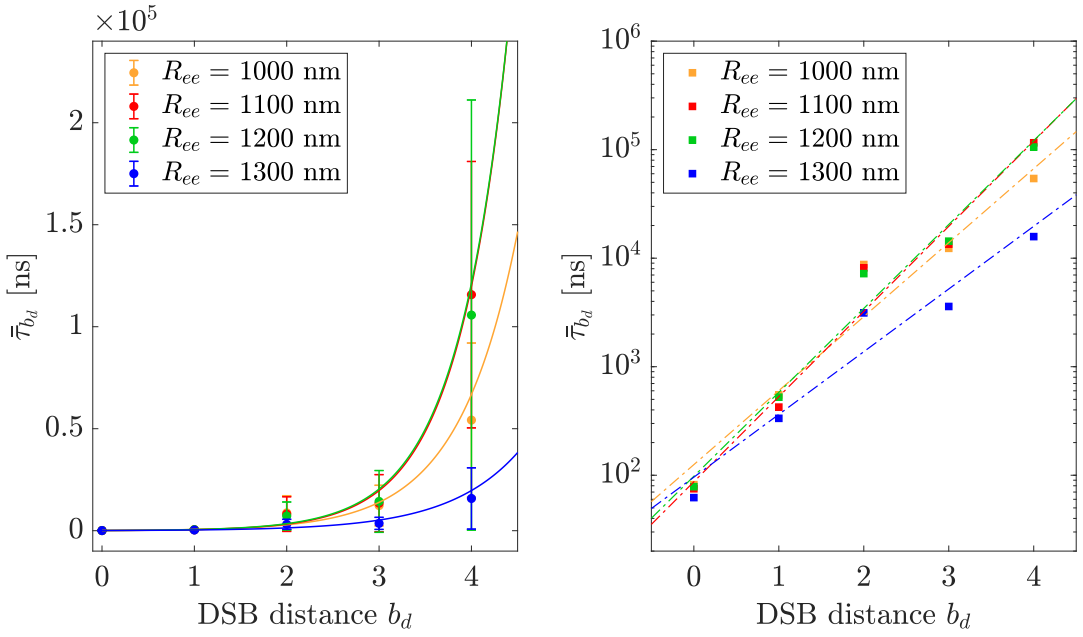

FIG. 4: Average fracture times $\bar{\tau}_{b_d}$ as function of the DSB distance b_d (shown in semi-logarithmic scale in the right panel). The solid and dashed lines correspond to the curves derived from the fitting protocol described by Eq. 5.

TABLE II: A and B coefficients from the exponential fitting of the average rupture times on the DSB distances (Equation 5) for each DNA extension.

R_{ee} [nm]	A [ns]	B
1000	1.6 ± 0.3	125 ± 89
1100	1.8 ± 0.2	87 ± 62
1200	1.8 ± 0.3	97 ± 62
1300	1.3 ± 0.3	96 ± 70

TABLE III: α and β coefficients from the linear fitting of the internal energy barrier of the DSB dislocation upon the DSB distance, as described in Eq. 6, at different steering regimes.

R_{ee} [nm]	α	β
1000	6.0 ± 0.8	7 ± 2
1100	6.6 ± 0.6	7 ± 2
1200	6.0 ± 0.6	8 ± 2
1300	5.7 ± 0.7	8 ± 2

In this work, we pursued an alternative approach: in fact, we propose a simplified depiction of the activated process by taking advantage of the peculiarities of the system at hand. Given $\Delta G^{\ddagger}$ as the height of the activation free energy barrier associated with the transition process from the bound (metastable) to the dislocated (stable) state (see Fig. 6), we have:

$$\Delta G^{\ddagger} = \Delta U^{\ddagger} - T\Delta S^{\ddagger} \tag{7}$$

where T is the temperature, and $\Delta U^{\ddagger}$ (or equivalently ΔU) and $\Delta S^{\ddagger}$ define the internal energy and entropic contributions, respectively. Since the steering protocol enforces a restraint on the conformational freedom of the DNA, it is reasonable to expect that the entropic contribution be constant up to the peak of the free energy barrier, thus leading to a cancellation of the entropic term and reducing Eq. 7 to:

$$\Delta G^{\ddagger} \approx \Delta U^{\ddagger} \tag{8}$$

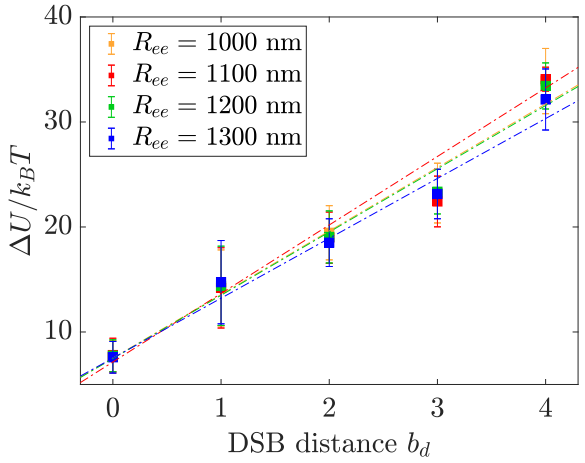

FIG. 5: Internal energy barriers associated with the dislocation of DSBs as a function of the distance b_d for each R_{ee} extension. The dashed curves are the results of the fitting protocol.

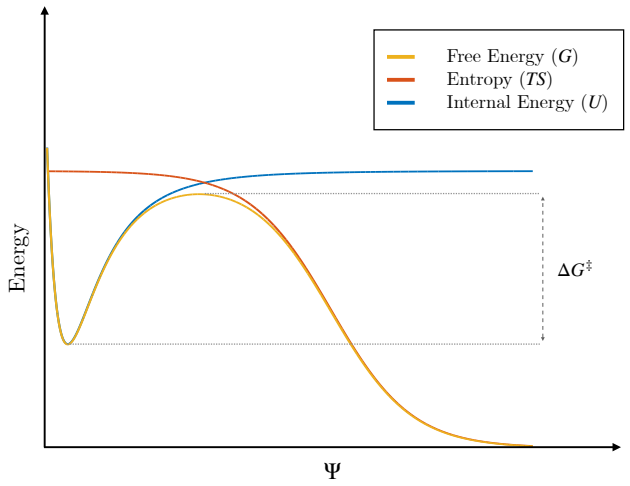

FIG. 6: Schematic representation of the free energy profile (yellow curve), associated with the rupturing process of DNA, as a function of an effective reaction coordinate Ψ. As a DSB of the covalent backbone is enforced, the DNA filament lies in a metastable state. Subject to a coaxial steering force of the DNA termini, it is reasonable to assume that the local conformational freedom of DNA is restrained: the main contribution to the activation free energy of the process is thus provided by the internal energy U (blue curve), while the entropic contribution TS is approximately constant (orange curve). This assumption holds up to the transition state between the two thermodynamic basins, separated by the activation energy $\Delta G^{\ddagger}$: In fact, as the DNA moieties are dislocated, several degenerate conformations become available, associated with a significant increase in the entropy of the system.

As the barrier is crossed, the DSB is dislocated and the DNA moieties acquire a significant conformational freedom, thereby increasing the entropy of the system. Fig. 6 schematically illustrates this process. These assumptions allow us to simplify the estimate of both the activation free energy of the process (since the forward activation barrier reduces to the internal energy difference provided by the fitting protocol) and of the characteristic times of the rupture of the DSB. In fact, the average rupture time for a DNA molecule damaged by a DSB motif and the activation free energy of the process are related *via* the Arrhenius-Kramers law as:

$$\bar{\tau}_{b_d} = \tau_0 \exp\left[\frac{\Delta G^{\ddagger}(b_d)}{k_B T}\right] \approx \tau_0 \exp\left[\eta \frac{\Delta U^{\ddagger}(b_d)}{k_B T}\right] \qquad (9)$$

where $\tau_0 = \tau_0(R_{ee})$ is the characteristic timescale of the activation process, which depends on the properties of the scenario at hand, such as the steering force. The η coefficient was here introduced to quantify the deviation from the actual empirical law.

Indeed, we verified that the kinetics of the DSB fracturing process is described by an exponential fit of the characteristic rupture times upon the free energy barrier of the dislocation, where τ_0 and η are the fitting coefficients. Fig. 7 shows the rupture time versus the activation free energy for each steered conformation; all coefficients from the fitting procedure are reported in Table IV.

Notably, the data shown in Fig. 7 corroborate the existence of an exponential correlation between $\bar{\tau}_{b_d}$ and $\Delta G^{\ddagger}$, in spite of significant error bars. This is in line with earlier *in silico* observations by Landuzzi and co-workers, who inferred an equivalent law from all-atom MD assessments [30]. Moreover, all (η, τ_0) coefficients are approximately equivalent, suggesting that the activation free energy depends on the DSB distance and negligibly on the steering protocol enforced (Fig. 5).

TABLE IV: Values of the η and τ_0 coefficients for each steered DNA conformation, as obtained by fitting the kinetic observables associated with the dislocation of the DSB motifs ($\Delta G^{\ddagger}/k_BT$, $\bar{\tau}$) *via* the Arrhenius-Kramers law (Eq. 9).

R_{ee} [nm]	η	τ_0 [ns]
1000	0.24 ± 0.04	26 ± 24
1100	0.27 ± 0.04	14 ± 13
1200	0.29 ± 0.05	12 ± 12
1300	0.23 ± 0.05	18 ± 20

Lastly, we extended the application range of the model to extrapolate the properties of DSB motifs at distances $b_d \geq 5$: Eqs. 6 and 9 were employed to infer the activation free energies and associated rupture times, as shown in Table V. By implying that the mechanical failure of DSBs is a two-step process, driven by the abrupt disruption of the residual contact interface between the DNA moieties, we associate a wide kinetic span (from 100 ns up to 0.3 s) to the fracturing process of DSB motifs at $b_d = 0 - 10$.

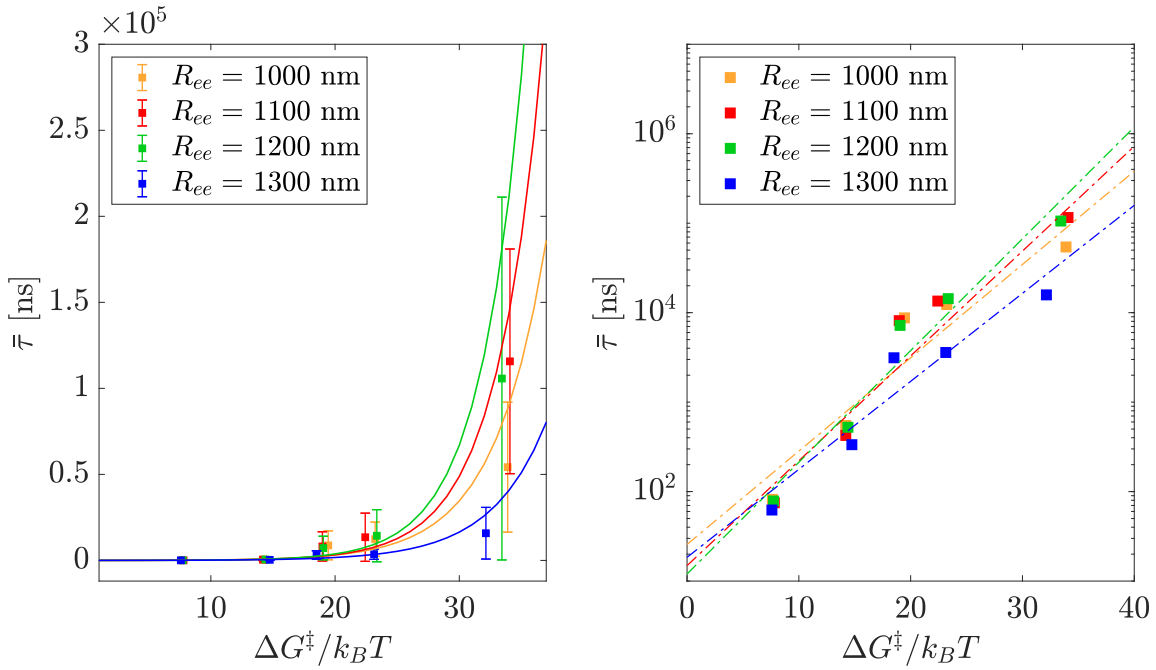

FIG. 7: Data from the kinetic assessment of the dislocation of DSB motifs ($\Delta G^{\ddagger}/k_BT$, $\bar{\tau}$) have been fitted by the Arrhenius-Kramers law (Eq. 9), for each steered DNA conformation. Results are shown in both linear and semi-logarithmic scale (the coefficients from the fitting protocol are listed in Table IV).

TABLE V: Extrapolated data of the activation free energies and rupture times of DSB motifs at distances $b_d > 4$, enforced on a linear 3855-bp DNA molecule at steered end-to-end distance $R_{ee} = 1000$ nm.

b_d	$\bar{\tau}$ [s]	$\Delta U^{\ddagger}/k_BT$
5	2×10^{-4}	38
6	1×10^{-3}	44
7	3×10^{-3}	50
8	1×10^{-2}	56
9	7×10^{-2}	62
10	3×10^{-1}	68

IV. DISCUSSION

In this work, we assessed the dynamical features of DNA double strand break (DSB) events and inferred the kinetics of the subsequent fracturing processes. As shown in Fig. 5, the internal energy barrier separating the bound (metastable) and fractured (stable) thermodynamic states increases linearly with the DSB distance b_d, i.e. the distance between the strand breaks of the DNA backbone. Moreover, the data show a negligible dependence of the internal energy barrier upon the steering protocol enforced on the DNA molecule. This assessment extends to DSB distances $b_d = 0 - 4$; beyond this value, we reasonably expect to observe an increasing deviation from a linear dependence of the height of the free energy barrier on the DSB distance.

Regarding the kinetics of the process, a few comments are in order. First and foremost, we observed a significant discrepancy between estimates of DSB rupturing times from CG and atomistic force-fields, associated with the dislocation of DSBs at distances $b_d \geq 2$ [30]. This might arise from a misestimate of the strength of non-covalent interactions by either model, accounting for slight artifacts in the depiction of nucleic acids by atomistic force-fields [31, 32, 55]. Yet, we remark that all inferences of the kinetics of the DSB rupturing process *in silico* are inherently bound and biased by the steering protocol enforced, as well as by the rescaling factor of the CG time step $\Gamma(\zeta)$. In cells, the dynamics of DSBs has been associated with a sub-diffusive regime, which is believed to apply to the chromatin ends of a DSB alike [29]. This fact suggests that a straightforward time rescaling protocol based on the ratio of the experimental and *in silico* diffusion coefficients of DNA might not be appropriate to depict the nuclear *milieu*. Nevertheless, these simulations establish an extensive benchmark of a single-molecule experimental setup.

Finally, we observe that the fitting of the characteristic times by the Arrhenius-Kramers law, Eq. 9, requires the introduction of a parameter $\eta < 1$. The origin of this discrepancy might lie in an overestimate of the height of the free energy barrier $\Delta U^{\ddagger}(b_d)$, and/or in the use of a top-down CG force-field, parameterized on equilibrium data, to assess an activated process: hence, we might reasonably expect that the timescales of the molecular dynamics deviate from those obtained by equilibrium proper-

ties. In fact, these results shine a spotlight on the quest to develop CG models that adequately incorporate the dynamical information to tackle the estimate of time-related observables.

V. CONCLUSIONS

Double strand breaks (DSBs), i.e. the twofold, close cleft of the DNA backbone on complementary strands, are a likely and detrimental outcome of the radiation field in cell nuclei. A dynamical characterisation of the local mechanical breakdown of DNA is critical, as it sets the stage for the subsequent cascade of events, involving the activation of the DNA damage repair machinery and the faithful or erroneous rejoining of the broken DNA moieties.

In this work, we addressed the *in silico* assessment of the early stages of the mechanical fracture of DNA as a consequence of DSBs enforced on a tensioned DNA filament. We performed extensive molecular dynamics simulations by means of a coarse-grained model of DNA, which let us cover biologically significant timescales, yet keeping a proper level of detail of the molecular processes. Namely, we established a robust, consistent protocol to estimate the characteristic timescales and activation barrier of the dislocation of the DSB motifs on DNA filaments tensioned between anchoring sites, depicting an OT experimental setup.

The internal energy barrier separating the bound (metastable) and fractured states exhibits a linear dependence with the DSB distance for all steered setups, suggesting that the residual base pairing holding the DNA moieties contributes to the contact energy in an additive manner within the distance range under scrutiny - that is $b_d = 0 - 4$; in fact, deviations from linearity might be expected at larger DSB distances ($b_d \geq 5$) on account of over-steering and/or over-twisting, long-range effects.

As for the kinetics of the DSB fracturing event, we observed an exponential increase of the average rupture times with the DSB distance, for all DSB motifs and steered end-to-end setups. This supports the depiction of the DSB-driven breakdown of a DNA filament as an activated process, where the system transitions from a metastable, bound state to a fractured state *via* the disruption of the residual interactions.

Building on these results, we estimated the free energy barrier separating the two states at each DSB distance, and associated their value to the average rupture times according to the Arrhenius-Kramers law. While this assumption overall holds, a deviation from the canonical formulation of the Arrhenius-Kramers law was observed, correcting the expected exponential behavior, likely accounting for the limitations in the CG model employed, either in the quantitative estimate of the energies involved or in the description of out-of-equilibrium processes - or both. This discrepancy calls for the development of coarse-grained models tailored on the specific characteristics of activated processes, and critically on the mechanics of DNA.

In conclusion, in this work we have verified the capabilities of simple and effective models of DNA in describing the phenomenology of radiation-induced DNA lesions, namely DNA double strand breaks, and acknowledged the limits of their validity. While further scrutiny is in order to fully characterise the early cascade of events following the collision of ionising radiation on cell nuclei, arguably the tools at our disposal are reliable and solid, paving the way for further developments.

SUPPLEMENTARY DATA

Supplementary Data are available.

DATA AVAILABILITY

The raw data associated with this work are freely available on a Zenodo repository at the link https://doi.org/10.5281/zenodo.6791939.

ACKNOWLEDGEMENTS

The authors wish to thank Roberto Menichetti and Luca Tubiana for a critical reading and insightful comments.

FUNDING

This project received funding from the European Research Council (ERC) under the European Union's Horizon 2020 research and innovation program (Grant 758588). RP and MM acknowledge support from the Italian Ministry of Education, University and Research (MIUR) through the FARE grant for the project HAMMOCK (Grant R18ZHWY3NC).

CONFLICT OF INTEREST STATEMENT.

None declared.

[1] Tomas Lindahl. Instability and decay of the primary structure of dna. *nature*, 362(6422):709–715, 1993.

[2] Rebecca A Burrell, Sarah E McClelland, David Endesfelder, Petra Groth, Marie-Christine Weller, Nadeem

Shaikh, Enric Domingo, Nnennaya Kanu, Sally M Dewhurst, Eva Gronroos, et al. Replication stress links structural and numerical cancer chromosomal instability. *Nature*, 494(7438):492–496, 2013.

[3] Agnes Schipler and George Iliakis. Dna double-strand–break complexity levels and their possible contributions to the probability for error-prone processing and repair pathway choice. *Nucleic acids research*, 41(16):7589–7605, 2013.

[4] Harvey Lodish and S Lawrence Zipursky. Molecular cell biology. *Biochem Mol Biol Educ*, 29:126–133, 2001.

[5] J. F. Ward. Dna damage produced by ionizing radiation in mammalian cells: identities, mechanisms of formation, and reparability. *Progress in Nucleic Acid Research and Molecular Biology*, 35:95–125, 1988.

[6] Dudley T Goodhead. Energy deposition stochastics and track structure: what about the target? *Radiation protection dosimetry*, 122(1-4):3–15, 2006.

[7] KM Prise, M Pinto, HC Newman, and BD Michael. A review of studies of ionizing radiation-induced double-strand break clustering. *Radiation research*, 156(5):572–576, 2001.

[8] Dudley T Goodhead. The initial physical damage produced by ionizing radiations. *International journal of radiation biology*, 56(5):623–634, 1989.

[9] GW Barendsen. The relationships between rbe and let for different types of lethal damage in mammalian cells: biophysical and molecular mechanisms. *Radiation research*, 139(3):257–270, 1994.

[10] G Iliakis, H Wang, AR Perrault, W Boecker, B Rosidi, F Windhofer, W Wu, J Guan, G Terzoudi, and G Pantelias. Mechanisms of dna double strand break repair and chromosome aberration formation. *Cytogenetic and genome research*, 104(1-4):14–20, 2004.

[11] Errol C Friedberg. Dna damage and repair. *Nature*, 421(6921):436–440, 2003.

[12] B Jakob, J Splinter, and G Taucher-Scholz. Positional stability of damaged chromatin domains along radiation tracks in mammalian cells. *Radiation research*, 171(4):405–418, 2009.

[13] Errol C Friedberg, Graham C Walker, Wolfram Siede, and Richard D Wood. *DNA repair and mutagenesis*. American Society for Microbiology Press, 2005.

[14] DJ Brenner and JF Ward. Constraints on energy deposition and target size of multiply damaged sites associated with dna double-strand breaks. *International journal of radiation biology*, 61(6):737–748, 1992.

[15] Emanuele Scifoni. Radiation biophysical aspects of charged particles: from the nanoscale to therapy. *Modern Physics Letters A*, 30(17):1540019, 2015.

[16] Konstantinos P Chatzipapas, Panagiotis Papadimitroulas, Dimitris Emfietzoglou, Spyridon A Kalospyros, Megumi Hada, Alexandros G Georgakilas, and George C Kagadis. Ionizing radiation and complex dna damage: Quantifying the radiobiological damage using monte carlo simulations. *Cancers*, 12(4):799, 2020.

[17] Eugene Surdutovich and Andrey V Solov'yov. Multiscale approach to the physics of radiation damage with ions. *The European Physical Journal D*, 68(11):1–30, 2014.

[18] Ervin B Podgoršak et al. *Radiation physics for medical physicists*, volume 1. Springer, 2006.

[19] H. Nikjoo, P. ONeill, D. T. Goodhead, and M. Terrissol. Computational modelling of low-energy electron-induced dna damage by early physical and chemical events. *International Journal of Radiation Biology*, 71(5):467–483, 1997.

[20] W. Friedland, M. Dingfelder, P. Kundrát, and P. Jacob. Track structures, dna targets and radiation effects in the biophysical monte carlo simulation code partrac. *Mutation Research/Fundamental and Molecular Mechanisms of Mutagenesis*, 711:28–40, 2011.

[21] N. Lampe, M. Karamitros, V. Breton, J. M. C. Brown, I. Kyriakou, D. Sakata, D. Sarramia, and S. Incerti. Mechanistic dna damage simulations in geant4-dna part 1: A parameter study in a simplified geometry. *Physica Medica*, 48:135–145, 2018.

[22] A Cucinotta, H Nikjoo, P O'Neill, and DT Goodhead. Kinetics of dsb rejoining and formation of simple chromosome exchange aberrations. *International journal of radiation biology*, 76(11):1463–1474, 2000.

[23] Werner Friedland, Peter Jacob, and Pavel Kundrát. Stochastic simulation of dna double-strand break repair by non-homologous end joining based on track structure calculations. *Radiation research*, 173(5):677–688, 2010.

[24] Werner Friedland and Pavel Kundrát. Track structure based modelling of chromosome aberrations after photon and alpha-particle irradiation. *Mutation Research/Genetic Toxicology and Environmental Mutagenesis*, 756(1-2):213–223, 2013.

[25] S Girst, V Hable, GA Drexler, C Greubel, C Siebenwirth, M Haum, AA Friedl, and G Dollinger. Subdiffusion supports joining of correct ends during repair of dna double-strand breaks. *Scientific reports*, 3(1):1–6, 2013.

[26] J. Miné-Hattab, V. Recamier, I. Izeddin, R. Rothstein, and X. Darzacq. Multi-scale tracking reveals scale-dependent chromatin dynamics after dna damage. *Molecular Biology of the Cell*, 28(23):3323–3332, 2017.

[27] Evi Soutoglou, Jonas F Dorn, Kundan Sengupta, Maria Jasin, Andre Nussenzweig, Thomas Ried, Gaudenz Danuser, and Tom Misteli. Positional stability of single double-strand breaks in mammalian cells. *Nature cell biology*, 9(6):675–682, 2007.

[28] W. Friedland, P. Jacob, and P. Kundrát. Mechanistic simulation of radiation damage to dna and its repair: on the track towards systems radiation biology modelling. *Radiation Protection Dosimetry*, 143:542548, 2011.

[29] John W Warmenhoven, Nicholas T Henthorn, Samuel P Ingram, Amy L Chadwick, Marios Sotiropoulos, Nickolay Korabel, Sergei Fedotov, Ranald I Mackay, Karen J Kirkby, and Michael J Merchant. Insights into the non-homologous end joining pathway and double strand break end mobility provided by mechanistic in silico modelling. *DNA repair*, 85:102743, 2020.

[30] Fabio Landuzzi, Pier Luca Palla, and Fabrizio Cleri. Stability of radiation-damaged dna after multiple strand breaks. *Physical Chemistry Chemical Physics*, 19(22):14641–14651, 2017.

[31] J. Yoo, D. Winogradoff, and A. Aksimentiev. Molecular dynamics simulations of dnadna and dnaprotein interactions. *Current Opinion in Structural Biology*, 64:88–96, 2020.

[32] Pablo D Dans, Jürgen Walther, Hansel Gómez, and Modesto Orozco. Multiscale simulation of dna. *Current opinion in structural biology*, 37:29–45, 2016.

[33] Jaakko J Uusitalo, Helgi I Ingólfsson, Parisa Akhshi, D Peter Tieleman, and Siewert J Marrink. Martini coarse-grained force field: extension to dna. *Journal of chemical theory and computation*, 11(8):3932–3945, 2015.

[34] Gordon S Freeman, Daniel M Hinckley, Joshua P Lequieu, Jonathan K Whitmer, and Juan J De Pablo. Coarse-grained modeling of dna curvature. *The Journal of chemical physics*, 141(16):10B615_1, 2014.

[35] Thomas E Ouldridge, Ard A Louis, and Jonathan PK Doye. Structural, mechanical, and thermodynamic properties of a coarse-grained dna model. *The Journal of chemical physics*, 134(8):02B627, 2011.

[36] Benedict EK Snodin, John S Schreck, Flavio Romano, Ard A Louis, and Jonathan PK Doye. Coarse-grained modelling of the structural properties of dna origami. *Nucleic acids research*, 47(3):1585–1597, 2019.

[37] Michelle D Wang, Hong Yin, Robert Landick, Jeff Gelles, and Steven M Block. Stretching dna with optical tweezers. *Biophysical journal*, 72(3):1335–1346, 1997.

[38] Thomas E Ouldridge. *Coarse-grained modelling of DNA and DNA self-assembly*. Springer Science & Business Media, 2012.

[39] Petr Šulc, Flavio Romano, Thomas E Ouldridge, Lorenzo Rovigatti, Jonathan PK Doye, and Ard A Louis. Sequence-dependent thermodynamics of a coarse-grained dna model. *The Journal of chemical physics*, 137(13):135101, 2012.

[40] Benedict EK Snodin, Ferdinando Randisi, Majid Mosayebi, Petr Šulc, John S Schreck, Flavio Romano, Thomas E Ouldridge, Roman Tsukanov, Eyal Nir, Ard A Louis, et al. Introducing improved structural properties and salt dependence into a coarse-grained model of dna. *The Journal of chemical physics*, 142(23):06B613_1, 2015.

[41] A. Sengar, T. E. Ouldridge, O. Henrich, L. Rovigatti, and P. Šulc. A primer on the oxdna model of dna: When to use it, how to simulate it and how to interpret the results. *Frontiers in Molecular Biosciences*, 8:551, 2021.

[42] Praveen K Depa and Janna K Maranas. Speed up of dynamic observables in coarse-grained molecular-dynamics simulations of unentangled polymers. *The Journal of chemical physics*, 123(9):094901, 2005.

[43] A. P. Thompson, H. M. Aktulga, R. Berger, D. S. Bolintineanu, W. M. Brown, P. S. Crozier, P. J. in 't Veld, A. Kohlmeyer, S. G. Moore, T. D. Nguyen, R. Shan, M. J. Stevens, J. Tranchida, C. Trott, and S. J. Plimpton. LAMMPS - a flexible simulation tool for particle-based materials modeling at the atomic, meso, and continuum scales. *Comp. Phys. Comm.*, 271:108171, 2022.

[44] Aidan P Thompson, H Metin Aktulga, Richard Berger, Dan S Bolintineanu, W Michael Brown, Paul S Crozier, Pieter J in't Veld, Axel Kohlmeyer, Stan G Moore, Trung Dac Nguyen, et al. Lammps-a flexible simulation tool for particle-based materials modeling at the atomic, meso, and continuum scales. *Computer Physics Communications*, 271:108171, 2022.

[45] Ruslan L Davidchack, TE Ouldridge, and MV Tretyakov. New langevin and gradient thermostats for rigid body dynamics. *The Journal of chemical physics*, 142(14):144114, 2015.

[46] Oliver Henrich, Yair Augusto Gutiérrez Fosado, Tine Curk, and Thomas E. Ouldridge. Coarse-grained simulation of dna using lammps. *The European Physical Journal E*, 41(5):57, 2018.

[47] JB Accary and Victor Teboul. Time versus temperature rescaling for coarse grain molecular dynamics simulations. *The Journal of chemical physics*, 136(9):094502, 2012.

[48] Masao Doi and Samuel Frederick Edwards. *The theory of polymer dynamics*, volume 73. oxford university press, 1988.

[49] Hauke Clausen-Schaumann, Matthias Rief, Carolin Tolksdorf, and Hermann E Gaub. Mechanical stability of single dna molecules. *Biophysical journal*, 78(4):1997–2007, 2000.

[50] Rae M Robertson, Stephan Laib, and Douglas E Smith. Diffusion of isolated dna molecules: dependence on length and topology. *Proceedings of the National Academy of Sciences*, 103(19):7310–7314, 2006.

[51] Mauro Ferrario, Giovanni Ciccotti, and Kurt Binder. *Computer Simulations in Condensed Matter: From Materials to Chemical Biology. Volume 1*, volume 703. Springer, 2007.

[52] Peter G Bolhuis, David Chandler, Christoph Dellago, and Phillip L Geissler. Transition path sampling: Throwing ropes over rough mountain passes, in the dark. *Annual review of physical chemistry*, 53(1):291–318, 2002.

[53] Phillip L Geissler, Christoph Dellago, and David Chandler. Kinetic pathways of ion pair dissociation in water. *The Journal of Physical Chemistry B*, 103(18):3706–3710, 1999.

[54] Christoph Dellago, Peter G Bolhuis, Félix S Csajka, and David Chandler. Transition path sampling and the calculation of rate constants. *The Journal of chemical physics*, 108(5):1964–1977, 1998.

[55] P. S. Nerenberg and T. Head-Gordon. New developments in force fields for biomolecular simulations. *Current Opinion in Structural Biology*, 49:129–138, 2018.